

# High efficiency photonic storage of single photons in cold atoms

Jianfeng Li<sup>1†</sup>, Yunfei Wang<sup>1†</sup>, Shanchao Zhang<sup>2†</sup>, Junyu He<sup>1</sup>, Aiqin Cheng<sup>1</sup>, Hui Yan<sup>1\*</sup>, and Shi-Liang Zhu<sup>3,1,4\*</sup>

<sup>1</sup>*Guangdong Provincial Key Laboratory of Quantum Engineering and Quantum Materials, SPTE, South China Normal University, Guangzhou 510006, China*

<sup>2</sup>*Department of Physics, The Hong Kong University of Science and Technology, Clear Water Bay, Kowloon, Hong Kong, China*

<sup>3</sup>*National Laboratory of Solid State Microstructures, School of Physics, Nanjing University, Nanjing 210093, China*

<sup>4</sup>*Synergetic Innovation Center of Quantum Information and Quantum Physics, University of Science and Technology of China, Hefei 230026, China*

(Dated: August 2, 2017)

An efficient quantum storage is highly desired for quantum information processing. As indicated by certain applications, a universal quantum storage is required to have a storage efficiency above 50% to beat the no-cloning limit. Although significant progress has been achieved in improving various quantum storage, the best storage efficiency of single photons is still below this criteria. By integrating a highly controllable single photon source with an optimized quantum storage, here we demonstrate an optical storage of single photons with storage efficiency of 65% in a cold atomic ensemble based on electromagnetically induced transparency. Meanwhile, the nonclassical characteristics of our storage are verified through the well-maintained nonclassical and single photon nature of the retrieved single photons.

## I. INTRODUCTION

A quantum storage (QS) that records quantum information, generally encoded in the quantum state of a qubit, for later on-demand retrieval is indispensable to the development of quantum information processing [1–6]. A single photon, the fundamental energy quanta of light, is the most promising candidate for the flying qubit that transmits the quantum information between quantum nodes. Therefore, an available QS of single photon lies at the heart of building up the large scale quantum network. Since the first demonstration of storing the quantum state of light in the material [7], many QS schemes based on coherent light-matter interaction have been proposed and successfully demonstrated [8, 9], such as electromagnetically induced transparency (EIT) [2, 7, 10–14, 16–20, 44], photon echo [21–24] and off-resonance Raman interaction [25–28].

An ideal QS must be capable of releasing a qubit in a lossless and quantum way after storing it for a controllable time. While certain loss and noises are inevitable in reality, a universal QS of photonic qubit must surpass the no-cloning limit [24] with storage efficiency (SE) above the threshold of 50% in many quantum applications. More practically, to implement the long-distance quantum communication, a larger SE would significantly improve the transmission rates [4, 5, 21].

In the past a few years, extraordinary progress has been made in improving the performance of QS of nonclassical light [11–14, 20–23, 28] and coherent light [10, 16–18, 24–27, 44]. Up to date, although the highest SE of above 90% has been successfully demonstrated with laser pulse [17] and the high SE of weak coherent pulse at single-photon level reaches 73% [24], the best SE of true single photons [13, 20, 22, 23, 28, 31–33] is still lower than the threshold. The main obstacle to realizing a higher SE of single photons lies at the difficulty of both optimizing the QS and integrating

the QS with the versatile single photon sources.

In this paper, we report a storage of heralded single photons with SE of 65% that is above the threshold for the first time. SE dependence on the controllable parameters of the storage, the optical depth and the control laser intensity, are explored and the strategy of optimizing these parameters to obtain the best SE are presented in detail. To achieve this high storage efficiency, we firstly built up a highly controllable single photons source with photon wavelength matching the storage. Secondly, to achieve the high optical depth, a magneto-optical trap (MOT) with large trapping volume is designed for the sake of better system robustness and greater duty cycle while comparing to the setups of spatial [13] and temporal [17] dark MOT. The dephasing rate of our storage is minimized by compensating the residual magnetic field. Photon noises are quelled by implementing both the spatial and spectrum filters. Eventually, we succeed in realizing an efficient storage of single photons and our work is an important step towards the practical applications of QS.

## II. EXPERIMENTAL SETUP AND SINGLE PHOTON GENERATION.

The experimental setup is sketched in Fig. 1. It consists of a source that generates heralded single photons from a cigar-shaped MOT (MOT1) and a OS that operated in a second cigar-shaped MOT (MOT2). To integrate the single photon source with our EIT-based OS in MOT2 of <sup>85</sup>Rb atoms, we use the same atoms with proper energy level configuration in MOT1 to generate heralded single photons via the backward spontaneous four-wave mixing (sFWM) process, which automatically matches the single photon wavelength to the working wavelength of OS. The whole experiment runs periodically with a repetition rate of 100 Hz. In each cycle, after 9.5 ms loading time, atoms in both MOT1 and MOT2 are prepared in the same ground state  $|1\rangle$ . Following that is a 0.5 ms single-photon generation and storage window.

Significantly different from the storage process in the

<sup>†</sup>These authors contributed equally to this work.

\*email: yanhui@sclu.edu.cn; slzhu@nju.edu.cn

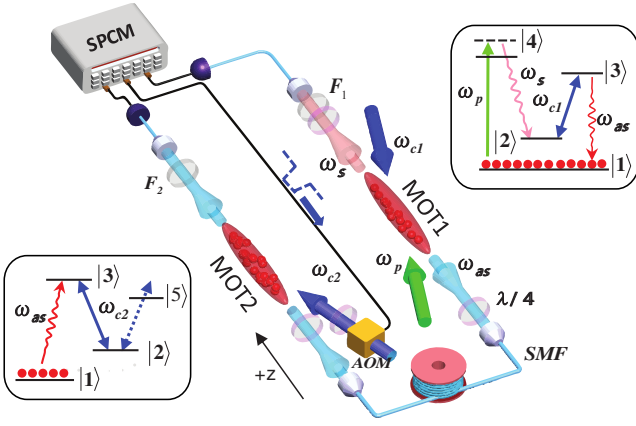


FIG. 1: (color online). Experimental setup: In MOT1, with the presence of a pump ( $\omega_p$ ) and coupling ( $\omega_{c1}$ ) lasers, counter-propagating Stokes ( $\omega_s$ ) and anti-Stokes ( $\omega_{as}$ ) paired photons are produced via the spontaneous four-wave-mixing (sFWM) process. The anti-Stokes photons ( $\omega_{as}$ ) are sent to MOT2 via a 100m long polarization-maintained single mode fiber (SMF). By switching off and on the control light ( $\omega_{c2}$ ) with an acousto-optic modulator (AOM), the photon can be stored into and readout from the electromagnetically induced transparency (EIT) based optical storage (OS) that operates in MOT2. The detailed  $^{85}\text{Rb}$  energy levels shown in the right inset for sFWM configuration and in the left inset for the EIT scheme are chosen as  $|1\rangle = |5S_{1/2}, F=2\rangle$ ,  $|2\rangle = |5S_{1/2}, F=3\rangle$ ,  $|3\rangle = |5P_{1/2}, F=3\rangle$ ,  $|4\rangle = |5P_{3/2}, F=3\rangle$ , and  $|5\rangle = |5P_{1/2}, F=2\rangle$ .  $\lambda/4$ : Quarter wave plates; SPCM: Single-photon counter module;  $F1$  and  $F2$ : Multi-level Fabry-Perot filters.

demonstrations using laser pulse[10, 17, 18, 24–27], storage of the heralded single photon in MOT2 is triggered by the detection of spontaneously generated Stokes photon, which requires the atomic ensemble property to stable during the storage window and hence our OS has an optimized duty cycle of 5% with the storage window of  $500\mu\text{s}$ . During this window, once a Stokes photon is detected, its paired anti-Stokes photon is projected into a single photon state as a heralded single photon and ready to be stored in MOT2.

### A. Heralded single photon generation.

To generate the heralded single photons, backward spontaneous four-wave-mixing (sFWM) configuration is implemented in MOT1 with longitudinal length  $L_1 = 1.5\text{ cm}$ , which includes a counter-propagating pump/coupling beam pair. The pump laser ( $780\text{ nm}, \sigma^-, \omega_p$ ) is a focusing beam with its focus point locating the center of MOT1 and has the frequency blue detuned from the transition  $|1\rangle \leftrightarrow |4\rangle$  by 80 MHz. The coupling laser ( $795\text{ nm}, \sigma^+, \omega_{c1}$ ) is a nearly collimated Gaussian beam with a  $1.8\text{ mm}$   $1/e^2$  diameter and has a frequency resonant with the transition  $|2\rangle \leftrightarrow |3\rangle$ . Phase-matched Stokes ( $\omega_s$ ) and anti-Stokes ( $\omega_{as}$ ) paired photons are produced along the longitudinal axis and coupled into two opposing single-mode fibers (SMFs). The two SMFs have mirrored spatial modes that both focus at the MOT1 center with

a  $0.24\text{ mm}$   $1/e^2$  diameter, which matches the spatial mode of the probe laser beam for measuring the longitudinal optical depth of MOT1. The angle between the Stokes/anti-Stokes axis and the pump/coupling axis is chosen to be  $2.5^\circ$ , which provides spatial separation of the weak Stokes and anti-Stokes fields from the strong pump and coupling fields. After a narrowband Fabry-Perot (FP) filter ( $F1$ ) with isolation ratio of 38 dB, the Stokes photons are detected by a single-photon counter module (SPCM, Perkin Elmer, SPCM-AQ4C) with a dark count rate of 500 counts per second.

A typical temporal waveform of the heralded single photons that are used in all the following OS experiments is shown in Fig. 2(a) (black open square), where the main wavepacket has a full width at half maximum (FWHM) around 400 ns. The sharp spike in the left of Fig. 1(a) is the optical precursor [35] that always propagates with light speed  $c_0$ . Taking into account the total channel efficiency (2.7%) and experiment duty cycle (5%), the single photon generation rate in the source is about 6400 photons per second. Here, the channel efficiency includes all the fiber coupling efficiency, the efficiency of optical filters and the detector efficiency of SPCM.

To produce single photons with above waveform, we set the optical depth of MOT1  $OD_1 = 100$  and Rabi frequency of the coupling laser  $\Omega_{c1} = 3.5\gamma_{13}$ , with  $\gamma_{13} = 2\pi \times 3.0\text{ MHz}$  being the electric dipole relaxation rate between states  $|1\rangle \leftrightarrow |3\rangle$ . The focused pump laser beam ( $\Omega_p$ ) is achieved by a plano-convex lens instead of the complicated spatial light modulator setup[34]. Its Rabi frequency is designed to have a spatial distribution of  $\Omega_p(z) = \Omega_{p0}f_p(z)$ , where  $\Omega_{p0} = 0.5\gamma_{13}$ ,  $f_p(z) = e^{-z^2/(4.16\text{mm})^2}$  and  $z = 0$  indicate the center of MOT1 (See supplement material). This spatial profile of pump laser makes the main part of the heralded single photon waveform a Gaussian shape as designed. The theoretical curve, shown in Fig. 2(a) (black line), can be calculated according to the following equation[34]:

$$\psi_{as}(\tau) = \kappa_0 V_{g1} f_p(L_1/2 - V_{g1}\tau) e^{-i\omega_{as}\tau}, \quad (1)$$

where  $\psi_{as}(\tau)$  is the wavepacket of heralded single photons with  $\tau$  as the relative time defined respect to the time instant when a Stokes photon is detected in each experiment period,  $\kappa_0$  is the nonlinear coupling strength of sFWM process, and  $V_{g1} = \Omega_{c1}^2 L_1 / (2OD_1 \gamma_{13})$  is the group velocity of the heralded single photon in MOT1.

The quantum nature of the generated photon can be verified with a Hanbury, Brown and Twiss interferometer that shows the non-separability of a single photon. A pure heralded single photon state promises  $g_c^{(2)} = 0$ , while a two-photon state gives  $g_c^{(2)} = 0.5$ . In our experiment, a finite measurement window  $t_W$  is taken to get a reasonable evaluation of  $g_c^{(2)}$ , as shown in the inset figure in 2(a). The definition of  $t_W$  of generated photons is respect to the Gaussian peak position of its own waveform. For reference, only the  $t_W$  of retrieved photon is depicted in 2(a). With a reasonable window, the generated shows a stable value  $g_c^{(2)} < 0.5$ . At a large enough window of  $t_W = 800\text{ ns}$ , we have  $g_c^{(2)} = 0.26 \pm 0.05$  with uncertainties derived from the Poisson statistics of the recorded photon

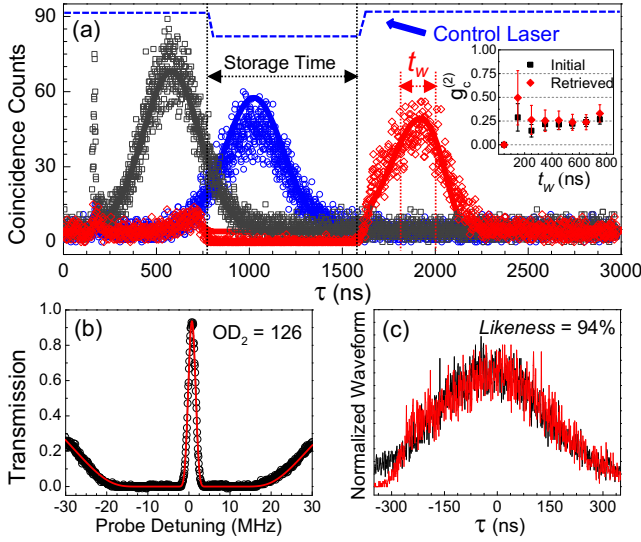


FIG. 2: (color online). (a) Typical temporal waveforms with total photon generation time of 3000 s. The measured initial, EIT-slowed and retrieved waveforms of heralded single photons are shown as black open square, blue open circle and red open diamond, while the theoretical curves are depicted as black, blue, and red lines, respectively. The dashed blue line indicates the temporal waveform of the control laser. The inset figure shows the typically measured conditional auto-correlation function  $g_c^{(2)}$  of the initial (red diamond) and retrieved photons (black square) when the measurement window  $t_w$  is changed around the peak of the respective Gaussian shape waveform. The error bars are obtained by considering the Poisson statistics of the photon counting. (b) The typical EIT transmission profile of the MOT2 with optical depth  $OD_2 = 126$ . Black open circles are experimental data and the red line is the best fitted theoretical curve. (c) Waveform likeness between the normalized temporal waveform of heralded single photon before and after storage.

counts, which strongly suggests a near-single-photon characteristic of generated photons. The nonclassical correlation between Stokes photon and anti-Stokes photon can be measured by the quantity of  $R_{CS} = g_{s,as}^2 / (g_{s,s}g_{as,as})$ [4], which means how many times the Cauchy-Schwarz inequality is violated. For our photon source, we have obtained a  $R_{CS} \approx 54$  around the peak of the main waveform.

### B. Optical storage setup.

A pair of opposing SMFs is setup in a way similar to that used for Stokes/anti-Stokes collection in MOT1 to deliver and collect the single photons through MOT2 with a longitudinal length of  $L_2 = 2.8$  cm. In each cycle, the quadruple gradient magnetic field in MOT2 is shut down in the last 1 ms of the atoms loading and state preparation period. During the storage window, a strong control laser ( $\omega_{c2}$ ) with a 4.7 mm  $1/e^2$  diameter and the same frequency as  $\omega_{c1}$  is switched on. The control laser ( $\Omega_{c2}$ ) can be switched off and on quickly with a switching time of 70 ns by an acousto-optic modulator (AOM) driven by a digital waveform generator (Rigol DSG815), which con-

trols the experiment timing of storing and read-out the single photon. The angle spanned by the single photon axis and the control laser axis is also chosen to be  $2.5^\circ$ . After passing through MOT2 and another 37 dB narrowband FP filter ( $F_2$ ), the heralded single photons are detected by a second SPCM (Perkin Elmer SPCM-AQRH-16FC) with a dark count rate of 25 counts per second. At last, the temporal waveforms of heralded single photons are recorded by a time-to-digital converter (Fast Comtec P7888) with a time bin resolution of 1 ns.

### III. STORAGE EFFICIENCY OPTIMIZATION AND NOISE SUPPRESSION.

SE of the storage of a single photon is defined as the ratio between the probability of successfully retrieving the single photon and the probability of a single photon being sent into the OS, i.e.,

$$SE = \frac{\int |\psi_{out}(\tau)|^2 d\tau}{\int |\psi_{in}(\tau)|^2 d\tau}, \quad (2)$$

where  $\psi_{in}$  ( $\psi_{out}$ ) is the wavepacket of the single photons before (after) the storage. The theoretical probabilities  $|\psi_{out}(\tau)|^2$  and  $|\psi_{in}(\tau)|^2$  can be derived by numerically solving Eqs.(3) detailed below. More practically, the well separated precursor part in  $\psi_{in}$  is excluded from the SE calculation because it cannot be slowed down and stored in the EIT scheme, which typically contributes less than 2% to the resulted SE.

#### A. Theoretical model of the EIT based storage

For guidance of the experimental optimization of the our OS, theoretical models[36, 38] based on the Maxwell-Schrodinger equation of single photon field and the optical Bloch equation of atomic ensembles are implemented to describe our storage, which is detailed below and has been demonstrated to work well with the EIT-based storage[17]:

$$\begin{aligned} (\partial_\tau + c_0 \partial_z) \tilde{\epsilon}_{as} &= ig\sqrt{N}\tilde{P} \\ \partial_\tau \tilde{P} &= -\gamma_{13}\tilde{P} + \frac{ig\sqrt{N}}{2}\tilde{\epsilon}_{as} + \frac{i}{2}\tilde{\Omega}_{c2}\tilde{S} \\ \partial_\tau \tilde{S} &= -\gamma_{12,eff}\tilde{S} + \frac{i}{2}\tilde{\Omega}_{c2}^*\tilde{P} \end{aligned} \quad (3)$$

where  $\tilde{\epsilon}_{as}$  is the time- and position- dependent slow varying envelop of the heralded single photon's quantum field and  $\tilde{\Omega}_{c2}$  is the Rabi frequency of the control laser.  $\tilde{P}$  and  $\tilde{S}$  are the slow varying envelope of the collective polarization of  $|1\rangle \leftrightarrow |3\rangle$  coherence and  $|1\rangle \leftrightarrow |2\rangle$  coherence, respectively.  $g$  is the photon-atom coupling strength and can be obtained from the relation  $OD_2 = g^2 NL_2 / (\gamma_{13}c_0)$ .  $N$  is the total atom number in the interaction volume with the assumption that atoms are distributed uniformly over MOT2.  $\gamma_{12,eff} = \gamma_{12} + \gamma_{13}(\beta\Omega_{c2})^2 / (4\Delta_s^2)$  is the effective dephasing rate of ground states  $|1\rangle \leftrightarrow |2\rangle$ , where  $\beta = \sqrt{37/50}$  is the Clebsch-Gordan coefficient ratio of  $|2\rangle \rightarrow |5\rangle$  transition

to the control laser transition, and  $\Delta_s = 2\pi \times 361.6$  MHz is the hyperfine excited state splitting between states  $|5\rangle$  and  $|3\rangle$  of  $^{85}\text{Rb}$  D1 lines. Here, the extra dephasing rate is introduced by the intense control laser that off-resonantly couples ground state  $|2\rangle$  to the excited state  $|5\rangle$ , which has spontaneous decay rate of  $2\gamma_{13}$ . With the anti-Stokes entrance position as  $\tilde{z} = 0$  in MOT2, we thus have  $\psi_{in}(\tau) = \psi_{as}(\tau)$  and  $\tilde{\epsilon}_{as}(\tau, \tilde{z} = 0) = \psi_{as}(\tau)e^{i\omega_{as}\tau}$ . After numerically solving Eq. (3) we obtain  $\tilde{\epsilon}_{as}(\tau, L_2)$  and then  $\psi_{out}(\tau)$  in the definition of SE in Eq. (2) can be derived from the relation  $\psi_{out}(\tau) = \tilde{\epsilon}_{as}(\tau, L_2)e^{-i\omega_{as}\tau}$ .

### B. Optimization of the single photon storage

Based on the above theoretical mode, the SE of our OS is mainly determined by the optical depth ( $OD_2$ ) of OS, the Rabi frequency ( $\Omega_{c2}$ ) of control laser and the dephasing rate ( $\gamma_{12}$ ) of the coherence between the two states  $|1\rangle$  and  $|2\rangle$ . We thus adopt the following protocol to optimize our OS: after preparing MOT2 with a certain optical depth  $OD_2$ , we reduce the value of  $\gamma_{12}$  in a way that will be detailed below.  $\Omega_{c2}$  is then scanned to optimize the SE of storing the single photon with a specific waveform. By repeating this procedure for another value of  $OD_2$ , we can obtain the optimal SE for all the experimentally reachable  $OD_2$ ,  $\gamma_{12}$  and  $\Omega_{c2}$ .

To achieve high enough optical depth  $OD_2$ , we increase the beam size of the trapping and repumping laser in MOT2 and hence expand the MOT2 trapping volume by more than 3 times. Eventually, we can tune the  $OD_2$  between 30 to 180 by adjusting the intensity of the repumping laser. The value of  $OD_2$  is measured separately by fitting the EIT transmission curve of a weak probe laser beam passing through MOT2 with the same spatial and polarization mode as that of the heralded single photon. The probe laser frequency is swept around the resonance of atomic transition  $|1\rangle \leftrightarrow |3\rangle$  with the control laser being continuously present. A typical EIT transmission curve with  $OD_2 = 126$  is shown in Fig.2(b).

With all the other parameters fixed, the SE is higher for a smaller  $\gamma_{12}$ . In our setup, finite inhomogeneous stray magnetic fields and atoms' residual thermal motion are two main contributions to  $\gamma_{12}$ . In order to minimize the magnetic field effect, we switch off the quadruple magnetic field and turn on three pairs of compensation Helmholtz coils during the storage window. The atomic motion effect is reduced by aligning the control laser beam properly with an optimal angle respect to the single photon path. The angle we choose at last is  $2.5^\circ$ , which is an empirical value in order to restrict the photon noise rate in the single photon channel to a safe level (90 photons per second) while maintaining feasible EIT transmission of the single photon. In addition, this angle is also large enough to effectively suppress the photon noise generation via nonlinear optical processes[17].

Finally, we measured the SE by scanning  $\Omega_{c2}$  with all the other settings unchanged. At each  $OD_2$ , a proper value of  $\Omega_{c2}$  that result in the optimal SE is obtained. Notably, to achieve optimal SE, it is desirable for the temporal waveform of a single photon to possess the time-reversal symmetry with the re-

trieved waveform [10, 37, 38]. In our OS, this statement is verified by the typically greater than 90% waveform likeness as shown in Fig.2(c), which will be further addressed below. Moreover, here we demonstrate an efficient way of matching the temporal mode of the OS to the input single photon waveform by simply adjusting the intensity of control laser.

## IV. CHARACTERISTICS OF THE STORAGE.

A typical optimal storage process and the resulted waveforms of the heralded single photon are illustrated in Fig.2(a) with  $OD_2 = 126$ . The retrieved waveform shown in Fig.2(a) (red open diamonds) has an SE of 62% with a storage time of 900 ns. As a reference, the waveform of the EIT-slowed single photon is also presented in Fig.2(a) (blue open circles) with an efficiency of 78%. The best fitted theoretical waveforms in Fig.2(a) (blue and red lines) are achieved with  $\Omega_{c2} = 7.6\gamma_{13}$  and  $\gamma_{12} = 0.004\gamma_{13}$ , where  $\Omega_{c2}$  and  $\gamma_{12}$  are free parameters during the fitting. In our theoretical calculation, effective dephasing rate  $\gamma_{12,eff}$  is used, which contains both the intrinsic  $\gamma_{12}$  and the extra dephasing rate induced by the off-resonant coupling between states  $|2\rangle \leftrightarrow |5\rangle$ . With the optimized SE, quantum properties of our OS are characterized by testing the quantum nature of the retrieved photons. Here, both the single photon nature and waveform likeness of the retrieved photons are measured.

### A. The nonclassical nature of OS.

The quantum nature of a single photon that can be evaluated by the auto-correlation function  $g_c^{(2)}$  is sensitive to the photon noises introduced by the OS during the storage. In our setup, most of the photon noises are from the scattering of the intense control laser beam by various optical elements. To suppress these noises, besides setting up a finite angle between the control laser beam and the single photon path, a single mode fiber (SMF) that acts as a spatial filter is used to collect the retrieved single photon. Furthermore, a set of temperature stabilized FP etalons are implemented as spectrum filters. Eventually, at  $t_w = 800\text{ns}$ , a safe vale of  $g_c^{(2)} = 0.32 \pm 0.09$  is measured for the retrieved photon, as presented in the figure and inset of Fig.2(a) (red open diamonds and red diamonds). Therefore, the single-photon nature of photons during the storage is well-preserved. On the other hand, the nonclassical correlation between retrieved photons and the Stokes photon are also preserved by measuring the  $R_{CS} \approx 29$  at the peak of the retrieved photon waveform. With these measurements, the nonclassical performance of our OS are well verified.

Waveform likeness is defined as the normalized cross correlation of two waveforms (See supplements). In the quantum applications that rely on the two-photon interference, the photon waveform also takes important role[4, 37]. As shown in Fig.2(c), the waveform likeness is around 94%, which demonstrates that the waveform is also preserved during the storage. We have to point out that, the waveform here does not bear any

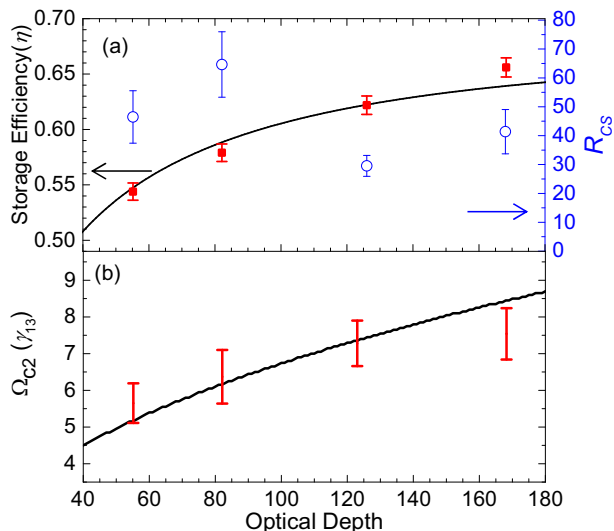


FIG. 3: (Color online). (a) Storage efficiency optimized for different optical depths ( $OD_2$ ). The efficiency data refers to the left axis. Error bars are based on the Poisson detection statistics and the black line is the theoretical curve. The nonclassical correlation between retrieved photon and the Stokes photon are denoted as blue open circle, which refers to the right axis. (b) Experimentally optimized Rabi frequency of control laser  $\Omega_{c2}$  at different  $OD_2$ . The uncertainty means a range where the storage efficiencies are indiscernible within the experimental fluctuations.

nonclassical nature. Moreover, since a Gaussian shape waveform has the intrinsic left-right symmetry, this high waveform likeness also implies the desired time-reversal symmetry [10, 37, 38] for an optimal SE.

### B. SE dependence on $OD_2$ and $\Omega_{c2}$

Following the theoretical prediction, the dependence of the optimal SE on  $OD_2$  are presented in Fig.3. At all  $OD_2$ 's, the optimal SE can be achieved with proper  $\Omega_{c2}$  values with the nonclassical properties of the retrieved photon preserved well. The red squares and blue open circles in Fig.3(a) are experiment data with error bars propagated from Poisson statistics of the measured photon counts under each  $OD_2$ . As predicted, SE continues to rise until it reaches the highest value around 65% at  $OD_2 = 168$ . Theoretical SEs are presented in Fig.3 (a) as a black line, which agrees well with the experimental data. Experimental values of optimal control laser Rabi frequency  $\Omega_{c2}$  at different  $OD_2$  are also tested and depicted in Fig.3(b), which show good agreement with the theoretical curve. Here the uncertainty reflects the range of  $\Omega_{c2}$  that gives a similar optimal SE within the experimental fluctuations.

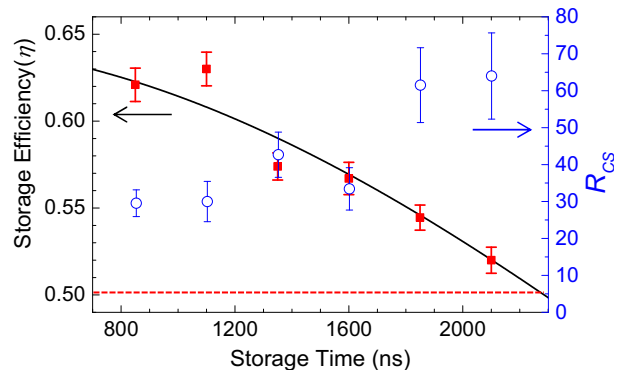


FIG. 4: (Color online). Storage efficiency (SE) with different storage times. Experimental data are denoted by red squares with error bars deducted from the Poisson detection statistics. The black line is the best fitted guideline with the Gaussian-decay function and the red dashed line show the SE of 50%. The nonclassical property of the retrieved photon are denoted as blue open circle that refer to the right axis.

### C. SE dependence on storage time

In practical application, a long enough storage time is required. Here, the SE dependence on different storage times is measured and depicted in Fig.4. The fractional delay, which is defined as the ratio of storage time to the initial waveform FWHM duration, is a useful evaluation in practical application. It predicts how many quantum unit operations can be conducted at most during the storage period and has a practically low limit of 1-bit. In Fig.4, the red squares are experimental SE measured at different storage times with  $OD_2 = 126$  and  $\Omega_{c2} = 7.6\gamma_{13}$ , the error bars are obtained by accounting for the Poisson statistics of measured photon counts. The black line is the best fit of the data with a Gaussian decay function[2, 17]  $e^{-t^2/\tau_0^2}$  that gives our storage coherence time of  $\tau_0 = 4 \mu s$ . With a typical SE of 50%, the storage time is  $2.2 \mu s$ , which gives a greater than 5-bit fractional delay with the SE above the 50%. Although, this is not a large value[24, 44], a large and promising improvement space can be expected with our current setups.

### V. CONCLUSION.

In conclusion, we have improved the storage efficiency of heralded single photons up to 65% in a dense cold atomic ensemble through the EIT scheme. With an SE of 50%, our OS reaches a storage time of  $2.2\mu s$ , which is more than a 5-bit fractional delay. As far as we know, this is the first demonstration of storing real single photons with efficiency above the 50% level. Here, we explore and demonstrate an feasible way of integration the single photon source and the optical memory, which would pave a way for seeking high efficiency storage of real single photon qubit. On the other hand, our progress would show a add up the confidence to the field in developing the practical quantum storage.

### Funding Information

NKRDP of China (Grants No. 2016YFA0301803 and No. 2016YFA0302800), the NSF of China (Grants No.

11474107, No. 61378012, No. 91636218), the GDSBPYS-TIT (Grant No.2015TQ01X715), the GNSFDYS (Grant No. 2014A030306012), the PRNPGZ (Grant No. 2014010).

- 
- [1] P.Kok, W. J. Munro, K. Nemoto, T. C. Ralph, J. P. Dowling, and G. J. Milburn, *Linear optical quantum computing with photonic qubits*, Rev. Mod. Phys. **79**, 135-174 (2007).
- [2] T. Chanelière, D. N. Matsukevich, S. D. Jenkins, S.-Y. Lan, T. A. B. Kennedy and A. Kuzmich, *Storage and retrieval of single photons transmitted between remote quantum memories*, Nature **438**, 833-836 (2005).
- [3] H. J. Kimble, *The quantum Internet*, Nature **453**, 1023-1030 (2008).
- [4] N. Sangouard, C. Simon, H. de Riedmatten, and N. Gisin, *Quantum repeaters based on atomic ensembles and linear optics*, Rev. Mod. Phys. **83**, 33-80 (2011).
- [5] F. Bussi eres, N. Sangouarda, M. Afzelius, H. de Riedmatten, C. Simond and W. Tittel, *Prospective applications of optical quantum memories*, J. Mod. Opt. **60**, 1519-1537 (2013).
- [6] L. M. Duan, M. D. Lukin, J. I. Cirac, and P. Zoller, *Long-distance quantum communication with atomic ensembles and linear optics*, Nature **414**, 413-418 (2001).
- [7] D. N. Matsukevich, and A. Kuzmich, *Quantum State Transfer Between Matter and Light*, Science. **306**, 663-666 (2004).
- [8] A. I. Lvovsky, B. C. Sanders, and W. Tittel, *Optical quantum memory*, Nat. Photonics **3**, 706-714 (2009).
- [9] K. Heshami, D. G. England, P. C. Humphreys, P. J. Bustard, V. M. Acosta, J. Nunn, and B. J. Sussman, *Quantum memories: emerging applications and recent advances*, J. Mod. Opt. **63**, 2005-2028 (2016).
- [10] I. Novikova, A. V. Gorshkov, D. F. Phillips, A. S. Sørensen, M. D. Lukin, and R. L. Walsworth, *Optimal control of light pulse storage and retrieval*, Phys. Rev. Lett. **98**, 243602 (2007).
- [11] J. Appel, E. Figueroa, D. Korystov, M. Lobino, and A. I. Lvovsky, *Quantum Memory for Squeezed Light*, Phys. Rev. Lett. **100**, 093602(2008).
- [12] H. Zhang, X.-M. Jin, J. Yang, H.-N. Dai, S.-J. Yang, T.-M. Zhao, J. Rui, Y. He, X. Jiang, F. Yang, G.-S. Pan, Z.-S. Yuan, Y. Deng, Z.-B. Chen, X.-H. Bao, S. Chen, B. Zhao, and J. -W. Pan, *Preparation and storage of frequency-uncorrelated entangled photons from cavity-enhanced spontaneous parametric downconversion*, Nat. Photonics **5**, 628-632 (2011).
- [13] S. Zhou, S. Zhang, C. Liu, J. F. Chen, J. Wen, M. M. T. Loy, G. K. L. Wong, and S. Du, *Optimal storage and retrieval of single-photon waveforms*, Opt. Express **20**, 24124-24131 (2012).
- [14] D.-S. Ding, Z.-Y. Zhou, B.-S. Shi, and G.-C. Guo, *Single-photon-level quantum image memory based on cold atomic ensembles*, Nat. Commun. **4**, 2527 (2013).
- [15] Y.-H. Chen, M.-J. Lee, I.-C. Wang, S. Du, Y.-F. Chen, Y.-C. Chen, and I. A. Yu, *Coherent Optical Memory with High Storage Efficiency and Large Fractional Delay*, Phys. Rev. Lett. **110**, 083601(2013).
- [16] D. Schraft, M. Hain, N. Lorenz, and T. Halfmann, *Stopped Light at High Storage Efficiency in a Pr<sup>3+</sup>:Y<sub>2</sub>SiO<sub>5</sub> Crystal*, Phys. Rev. Lett. **116**, 073602(2016)
- [17] Y.-F. Hsiao, P.-J. Tsai, H.-S. Chen, S.-X. Lin, C.-C. Hung, C.-H. Lee, Y.-H. Chen, Y.-F. Chen, I. A. Yu, Y.-C. Chen, *EIT-based photonic memory with near-unity storage efficiency*, arXiv:1605.08519 (2016).
- [18] L. Chen, Z. Xu, W. Zeng, Y. Wen, S. Li, and H. Wang, *Controllably releasing long-lived quantum memory for photonic polarization qubit into multiple spatially-separate photonic channels*, Sci. Rep. **6**, 33959 (2016).
- [19] M. Fleischhauer, A. Imamoglu, and J. P. Marangos, *Electromagnetically induced transparency: Optics in coherent media*, Rev. Mod. Phys. **77**, 633-673(2005).
- [20] M. Lettner, M. Mucke, S. Riedl, C. Vo, C. Hahn, S. Baur, J. Bochmann, S. Ritter, S. Durr, and G. Rempe, *Remote Entanglement between a Single Atom and a Bose-Einstein Condensate*, Phys. Rev. Lett. **106**, 210503 (2011).
- [21] M. P. Hedges, J. J. Longdell, Y. Li, and M. J. Sellars, *Efficient quantum memory for light*, Nature **465**, 1052-1056 (2010).
- [22] F. Bussi eres, C. Clausen, A. Tiranov, B. Korzh, V. B. Verma, S. W. Nam, F. Marsili, A. Ferrier, P. Goldner, H. Herrmann, C. Silberhorn, W. Sohler, M. Afzelius, and N. Gisin, *Quantum teleportation from a telecom-wavelength photon to a solid-state quantum memory*, Nat. Photonics **8**, 775-778 (2014).
- [23] E. Saglamyurek, J. Jin, V. B. Verma, M. D. Shaw, F. Marsili, S. W. Nam, D. Oblak, and W. Tittel, *Quantum storage of entangled telecom-wavelength photons in an erbium-doped optical fibre*, Nat. Photonics **9**, 83-87 (2015).
- [24] Y.-W. Cho, G. T. Campbell, J. L. Everett, J. Bernu, D. B. Higginsbottom, M. T. Cao, J. Geng, N. P. Robins, P. K. Lam, and B. C. Buchler, *Highly efficient optical quantum memory with long coherence time in cold atoms*, Optica **3**, 100-107(2016).
- [25] K. F. Reim, J. Nunn, V. O. Lorenz, B. J. Sussman, K. C. Lee, N. K. Langford, D. Jaksch, and I. A. Walmsley, *Towards high-speed optical quantum memories*, Nat. Photonics **4**, 218-221 (2010).
- [26] H. P. Specht, C. Nölleke, A. Reiserer, M. Uphoff, E. Figueroa, S. Ritter, and G. Rempe, *A single-atom quantum memory*, Nature **473**, 190-193 (2011).
- [27] D. J. Saunders, J. H. D. Munns, T. F. M. Champion, C. Qiu, K. T. Kaczmarek, E. Poem, P. M. Ledingham, I. A. Walmsley, and J. Nunn, *Cavity-Enhanced Room-Temperature Broadband Raman Memory*, Phys. Rev. Lett. **116**, 090501 (2016).
- [28] D.-S. Ding, W. Zhang, Z.-Y. Zhou, S. Shi, B.-S. Shi, and G.-C. Guo, *Raman quantum memory of photonic polarized entanglement*, Nat. Photonics **9**, 332-338(2015).
- [29] F. Grosshans, and P. Grangier, *Quantum cloning and teleportation criteria for continuous quantum variables*, Phys. Rev. A **64**, 010301 (2001).
- [30] M. Varnava, D. E. Browne, and T. Rudolph, *Loss tolerance in one-way quantum computation via counterfactual error correction*, Phys. Rev. Lett. **97**, 120501 (2006).
- [31] J. Jin, E. Saglamyurek, M. li G. Puigibert, V. Verma, F. Marsili, S. W. Nam, D. Oblak, and W. Tittel, *Telecom-Wavelength Atomic Quantum Memory in Optical Fiber for Heralded Polarization Qubits*, Phys. Rev. Lett. **115**, 140501 (2015).
- [32] J. Rui, Y. Jiang, S.-J. Yang, B. Zhao, X.-H. Bao, and J.-W. Pan, *Operating Spin Echo in the Quantum Regime for an Atomic-Ensemble Quantum Memory*, Phys. Rev. Lett. **115**, 133002 (2015).
- [33] D.-S. Ding, W. Zhang, Z.-Y. Zhou, S. Shi, J.-S. Pan, G.-Y. Xi-

- ang, X.-S. Wang, Y.-K. Jiang, B.-S. Shi, and G.-C. Guo, *Toward high-dimensional-state quantum memory in a cold atomic ensemble*, Phys. Rev. A **90**, 042301 (2014).
- [34] L. Zhao, X. Guo, Y. Sun, Y. Su, M. M. T. Loy, and S. Du, *Shaping the Biphoton Temporal Waveform with Spatial Light Modulation*, Phys. Rev. Lett. **115**, 193601 (2015).
- [35] S. Zhang, J. F. Chen, C. Liu, M. M. T. Loy, G. K. L. Wong, and S. Du, *Optical precursor of a single photon*, Phys. Rev. Lett. **106**, 243602 (2011).
- [36] M. Fleischhauer, and M. D. Lukin, *Dark-State Polaritons in Electromagnetically Induced Transparency*, Phys. Rev. Lett. **84**, 5094 (2001).
- [37] I. Novikova, N. B. Phillips, and A. V. Gorshkov, *Optimal light storage with full pulse-shape control*, Phys. Rev. A. **78**, 021802R (2008).
- [38] A. V. Gorshkov, A. André, M. Fleischhauer, A. S. Sørensen, and M. D. Lukin, *Universal approach to optimal photon storage in atomic media*, Phys. Rev. Lett. **98**, 123601 (2007).
- [39] L. Zhao, Y. Su, and S. Du, *Narrowband biphoton generation in the group delay regime*, Phys. Rev. A **93**, 033815 (2016).
- [40] L. Zhao, X. Guo, Y. Sun, Y. Su, M. M. T. Loy, and S. Du, *Shaping the Biphoton Temporal Waveform with Spatial Light Modulation*, Phys. Rev. Lett. **115**, 193601 (2015).
- [41] P. Grangier, G. Roger, and A. Aspect, *Experimental Evidence for a Photon Anticorrelation Effect on a Beam Splitter: A New Light on Single-Photon Interferences*, Europhys. Lett. **1**, 173(1986)
- [42] S. Zhang, J. F. Chen, C. Liu, M. M. T. Loy, G. K. L. Wong, and S. Du, "Optical precursor of a single photon," Phys. Rev. Lett. **106**, 243602 (2011)
- [43] P. Chen, C. Shu, X. Guo, M. M. T. Loy, and S. Du, "Measuring the biphoton temporal wave function with polarization-dependent and time-resolved two-photon interference," Phys. Rev. Lett. **114**, 010401 (2015);
- [44] Y.-H. Chen, M.-J. Lee, I.-C. Wang, S. Du, Y.-F. Chen, Y.-C. Chen, and T. A. Yu, *Coherent Optical Memory with High Storage Efficiency and Large Fractional Delay*, Phys. Rev. Lett. **110**, 083601(2013).

## VI. SUPPLEMENT MATERIALS

### A. Waveform shaping of heralded single photon

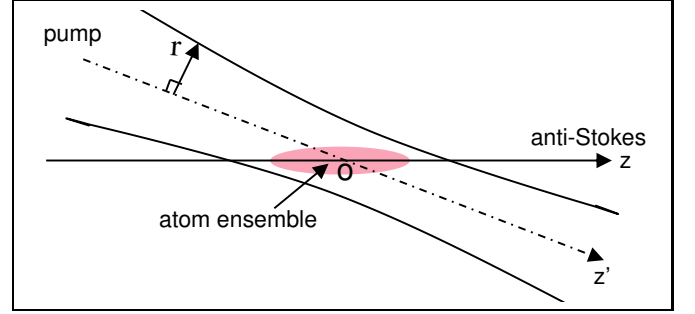


FIG. 5: Schematics describing the waveform shaping technique by controlling the pump beam profile.  $z$  axis is the longitudinal axis of the atom ensemble (MOT1) and the direction along which the Stokes and anti-Stokes pair are generated.  $z'$  is the propagation direction of pumping light with  $r$  as the beam radius of pumping beam in the transverse plane.

Here we show the details of how the desired temporal waveform of the heralded single photons can be achieved with the scheme presented in Ref[40]. The temporal waveform of single photon generated by the spontaneous four-wave-mixing (sFWM) process is determined simultaneously by the optical depth( $OD_1$ ), pump laser Rabi frequency  $\Omega_p$  and coupling laser Rabi frequency  $\Omega_{c1}$ [39, 40], with all the parameter definition following the main text. According to the discussion in Ref.[39], our photon source performs in the group delay regime and waveform generated photons are dominated by the group delay effects, which is the starting point to implement this spatial-temporal modulation technique. By intentionally preparing the coupling laser as a near collimated beam with large enough beam size, the generated temporal waveform are mainly determined by the carefully focused pumping beam with a designed spatial distribution of its Rabi frequency along the  $z$  axis, as depicted in Fig.5. Here, the distribution of pump laser Rabi frequency can be described as  $\Omega_p(z) = \Omega_{p0}f_p(z)$ , and the envelop of the temporal waveform of emitted single photon can be approximately given as:

$$\tilde{\psi}_{as}(\tau) \approx \kappa_0 \int_{-\frac{L_1}{2}}^{\frac{L_1}{2}} dz f_p(z) \int d\omega g_\chi^{(3)}(\omega) e^{-i\omega(\tau + \frac{z}{V_{g1}} - \tau_g)} \quad (4)$$

with  $\kappa_0 = \frac{\sqrt{\omega_{s0}\omega_{as0}}}{i4\pi c} \frac{\hbar^2 \Omega_{p0} \Omega_{c1}}{\mu_{14}\mu_{23}} \chi_0^{(3)}$  as the nonlinear coupling strength of. Here,  $c$  is the speed of light in vacuum,  $\hbar$  is the reduced Planck constant.  $\omega_{s0}/\omega_{as0}$  is the central frequency of Stokes/anti-Stokes photon,  $\mu_{ij}$  is the dipole matrix element between the state of  $|i\rangle$  and  $|j\rangle$  as the energy level shown in main text.  $\chi_0^{(3)}$  is the resonant 3rd order susceptibility and  $g_\chi^{(3)}(\omega)$  is the 3rd order susceptibility spectrum divided by  $\chi_0^{(3)}$ .  $V_{g1} = \frac{\Omega_{c1}^2 L_1}{(2OD_1 \gamma_{13})}$  is the group velocity of the anti-Stokes photons as defined in the main text and  $\tau_g = \frac{L_1}{V_{g1}}$ .  $\tau = \tau_{as} - \tau_s$  is the time interval between anti-Stokes photon and Stokes photon.

With the of integration variable change from  $z$  to  $t$  as  $t = \tau + \frac{z}{V_{g1}} - \tau_g$ , integration in the space domain in Eq. (S1) changes to integration in the time domain:

$$\tilde{\psi}_{as}(\tau) \approx \kappa_0 \int_{\tau-\tau_g}^{\tau} dt f_p\left(\frac{L_1}{2} + V_{g1}(t - \tau)\right) \times \int d\omega g_{\chi}^{(3)}(\omega) e^{-i\omega t} \quad (5)$$

In the group delay regime only the spectrum part near the EIT resonance plays the role in the integration about  $\omega$  due to the narrow EIT window, we thus can safely make the approximation  $g_{\chi}^{(3)}(\omega) \approx g_{\chi}^{(3)}(0) = 1$  and thus Eq. (S2) reduces to

$$\begin{aligned} \tilde{\psi}_{as}(\tau) &\approx \kappa_0 \int_{\tau-\tau_g}^{\tau} dt f_p\left(\frac{L_1}{2} + V_{g1}(t - \tau)\right) \delta(t) \\ &= \kappa_0 V_{g1} f_p\left(\frac{L_1}{2} - V_{g1}\tau\right) \end{aligned} \quad (6)$$

Hence, up to here, we briefly show the derivation of the envelope part of Eq.(1) in the main text. Considering the situation that  $f_p(z)$  has a Gaussian shape as below:

$$f_p(z) = e^{-\frac{z^2}{z_0^2}} \quad (7)$$

we will directly obtain an Gaussian shape temporal waveform as:

$$\tilde{\psi}_{as}(\tau) = \kappa_0 V_{g1} e^{-\frac{(\tau-\tau_g/2)^2}{\tau_0^2}} \quad (8)$$

with  $\tau_0 = \frac{z_0}{V_g} = \frac{z_0}{L_1} \tau_g$ .

In our setup, a lens is used to focus the pump laser on the center of the atom cloud, with the Rayleigh length is much longer than the length of the ensemble, the Rabi frequency along the  $z$  axis is thus

$$\Omega_p(r, z') = \Omega_p \frac{w_0}{w(z')} e^{-\frac{r^2}{w^2(z')}} \approx \Omega_p e^{-\frac{r^2}{w_0^2}} \quad (9)$$

Here  $w_0$  is the waist of the Gaussian beam, and  $z'$  is the direction of propagation. As shown in Fig. 5 the angle between the  $z$  and  $z'$  is chosen to be  $2.5^\circ$ , Thus the we have:

$$f_p(z) = e^{-\frac{(z \sin \theta)^2}{w_0^2}} \approx e^{-\frac{z^2}{(w_0/\theta)^2}} \quad (10)$$

Then we have

$$\tau_0 = \frac{2OD_1\gamma_{13}}{\Omega_{c1}^2 L_1} z_0 = \frac{2OD_1\gamma_{13}}{\Omega_{c1}^2 L_1 \theta} w_0 \quad (11)$$

According to Eq. (S8), we can easily control the width of the gaussian shape biphoton waveform by changing the  $OD_1$ ,  $\Omega_{c1}$  or  $w_0$ . In order to a high generation rate, generally we do not change the  $OD_1$ . As we mention in the main text, the parameters of our system are  $OD_1 = 100$ ,  $\gamma_{13} = 2\pi \times 3MHz$ ,  $L_1 = 1.5cm$  and  $\Omega_{c1} = 3.5\gamma_{13}$ . The focus of the lens we use has a focal length of 8mm and the distance between the lens and the center of the ensemble is about 70cm. With the waist of the fiber core  $w_{fiber} \approx 2.5\mu m$ , we have  $w_0 \approx 182\mu m$  and thus  $\tau_0 \approx 240ns$ . The full width of half maximum(FWHM) of the shaped biphoton waveform

is  $FWHM = 2\tau_0 \sqrt{\ln 2} \approx 400ns$ , just as we show in the paper. The Rabi frequency distribution of the pump laser a long  $z$  axis is thus fitted as:

$$f_p(z) \approx e^{-\frac{z^2}{(w_0/\theta)^2}} = e^{-\frac{z^2}{(4.16mm)^2}} \quad (12)$$

We thus can conclude that a single lens is stable and powerful enough for Gaussian type shaping and a spatial light modulator(SLM) might be necessary for more complicated shaping.

## B. Measurement of the conditional auto-correlation function

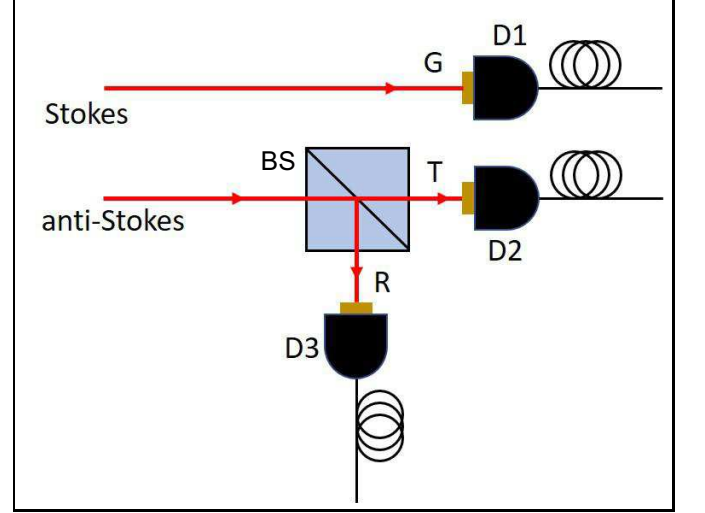


FIG. 6: Experimental setup for measuring the conditional autocorrelation function  $g_c^{(2)}$ .

The single-photon quantum nature can be verified by measuring the conditional auto-correlation function  $g_c^{(2)}$  of the anti-Stokes photon using a standard Hanbury-Brown-Twiss (HBT) interferometer [41]. The experimental set up of this measurement is shown in Fig. 6. The beam splitter (BS) used here has a half-half splitting ration with T and R denoting the transmission and reflection ports. D1, D2 and D3 are three single photon detectors that record the click event triggered by the photon in channel G, T and R, respectively. Definition of the conditional second-order auto-correlation function is [41]

$$g_c^{(2)} = P(TR|G)/[P(T|G)P(R|G)] \quad (13)$$

where  $P(R|G)$ ,  $P(T|G)$  and  $P(TR|G)$  are the conditional events probability, after the detector D1 click, of detector D2 click, detector D3 click and both detectors click at the same time, respectively. With the relation that  $P(X|G) = N(X)/N(G)$ , we have the following relation:

$$g_c^{(2)} = N(G)N(GTR)/[N(GT)N(GR)] \quad (14)$$

where  $N(G)$ ,  $N(GR)$ ,  $N(GT)$  and  $N(GTR)$  are D1 click counts, D1-D2 2-photon coincidence counts, D1-D3 2-photon coincidence counts and D1-D2-D3 3-photon coincidence



counts, respectively. Here we can see that for anti-Stokes photon in ideal single photon state we have  $g_c^{(2)} = 0$  and in the pure 2-photon state we have  $g_c^{(2)} = 0.5$ , thus in reality we may require the final  $g_c^{(2)} < 0.5$  as the criterion for the single photon source.

For a anti-Stokes photon, after sent onto a 50/50 beam splitter, it can be transmitted or reflected into the path T and path R with equal length and then finally be detected by single photon detectors placed in the transmission (D2) and reflection path (D3). Here, when there is a click in the Stokes photon channel(D1), the photon click events in both D2 and D3 with the time lapse ( $t_T$  and  $t_R$ ) relative to the click of Stokes photon will be recorded. To measure the  $g_c^{(2)}$  at zero delay,  $t_T = t_R$  must be hold in our time resolution. If at  $t_T = t_R$ , a coincidence count was recorded between D2 and D3, we treat it as a non-single photon event.

In reality, however, to make this measurement more safe, any coincidence count within a reasonable window defines as  $\Delta t_w > |t_T - t_R|$  will be treated as non-single photon. Therefore, in the Fig.(2) of main text, the  $g_c^{(2)}$  with different  $t_w$  are measured and presented to show the good single photon quality of both the photons from the source and the photons retrieved from the storage.

### C. Waveform likeness

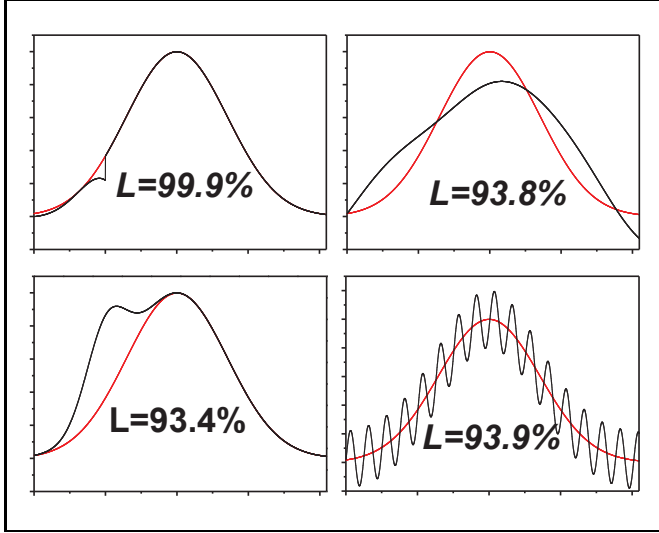


FIG. 7: Fake curves shown how sensitively does the defined likeness depend on the waveform shape .

The classical fidelity [44] is defined by

$$F_{class} = \frac{|\int E_{in}^*(t-t_d)E_{out}(t)dt|^2}{[\int |E_{in}(t)|^2dt][\int |E_{out}(t)|^2dt]} \quad (15)$$

Similarly, for a quantitative estimation, we calculate the temporal waveform likeness with the following definition:

$$L = \frac{|\int \psi_{in}^*(\tau-\tau_{delay})\psi_{out}(\tau)d\tau|^2}{[\int |\psi_{in}(\tau)|^2d\tau][\int |\psi_{out}(\tau)|^2d\tau]} \quad (16)$$

According to Ref[42, 43],  $\psi_{in}(\tau) = \sqrt{G_{in}^{(2)}(\tau)}$  and  $\psi_{out}(\tau) = \sqrt{G_{out}^{(2)}(\tau)}$  are reasonable approximations with  $G_{in}(\tau)$  and  $G_{out}(\tau)$  are Glauber correlation function before and after storage. Therefore, with waveform likeness  $L$  can be defined as :

$$L = \frac{|\sum \sqrt{N_{in}(\tau-\tau_{delay})N_{out}(\tau)}|^2}{\sum |\sqrt{N_{in}(\tau-\tau_{delay})}|^2 \times \sum |\sqrt{N_{out}(\tau-\tau_{delay})}|^2} \quad (17)$$

with  $N_{in/out}(\tau) = \eta_{channel}G_{in/out}^{(2)}(\tau)\Delta t_{bin}T$ . Here  $\eta_{channel}$  is the total channel efficiency,  $\Delta t_{bin}$  is the time bin and  $T$  is the total photon generation time. To give an intuitive impression about this value, we show a few fake curves in Fig.?? that testing how sensitive this quantity can be used to tell the waveform similarity.